







Effect of Pd and Cu co-catalyst on the charge carrier trapping, recombination and transfer during photocatalytic hydrogen evolution over WO₃-TiO₂ heterojunction

David Ramírez-Ortega^{1,*} , Diana Guerrero-Araque² , Próspero Acevedo-Peña³ , Luis Lartundo-Rojas⁴, and Rodolfo Zanella^{1,*} 

¹Instituto de Ciencias Aplicadas y Tecnología, Universidad Nacional Autónoma de México, Circuito Exterior S/N, Ciudad Universitaria, 04510 Mexico City, Mexico

²CONACYT-Universidad Autónoma Metropolitana, Departamento de Química, Av. San Rafael Atlixco 156, 09340 Mexico City, Mexico

³CONACYT-Instituto Politécnico Nacional, CICATA Legaria, 11500 Mexico City, Mexico

⁴Instituto Politécnico Nacional, Centro de Nanociencias y Micro y Nanotecnología, Zacatenco, Mexico City, Mexico

Received: 4 July 2020

Accepted: 29 August 2020

Published online:

9 September 2020

© Springer Science+Business Media, LLC, part of Springer Nature 2020

ABSTRACT

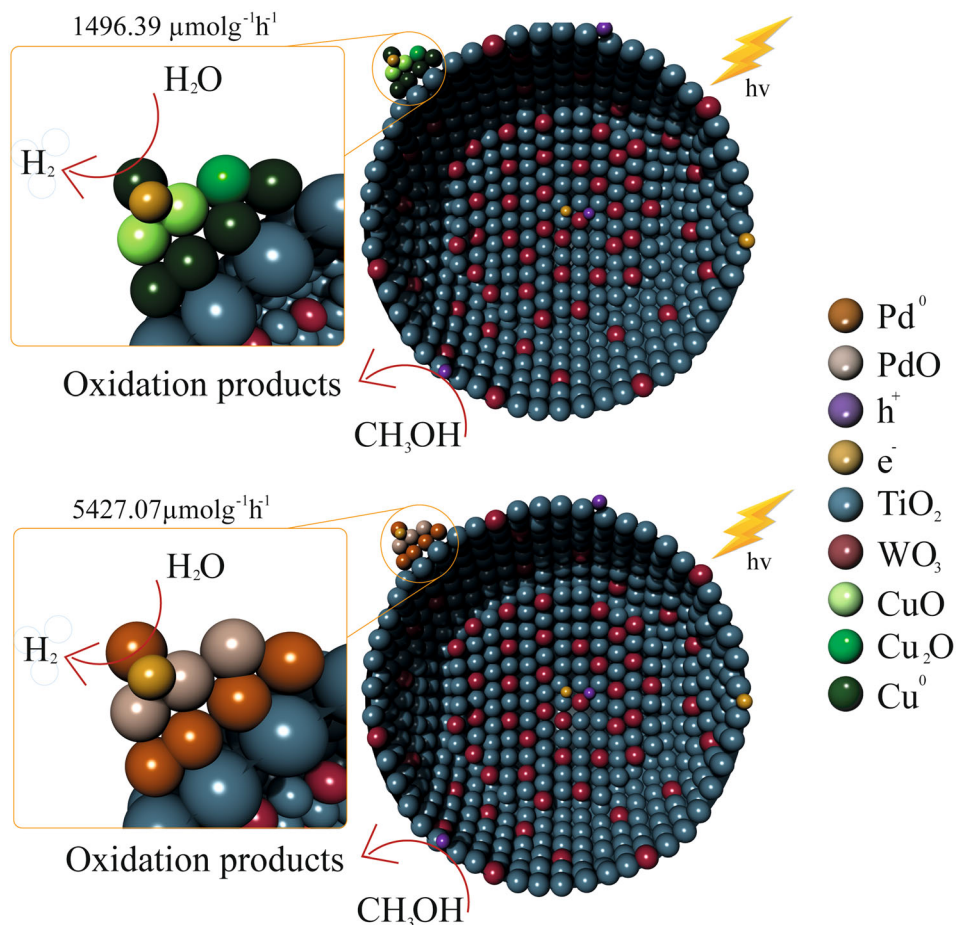
Co-catalysts are well known for improving the charge carrier's separation and transfer to species in solution, and hence, the photocatalytic hydrogen production. Thus, in this work, the effect of loading Cu and Pd species over the WO₃-TiO₂ structure was evaluated. The structure of WO₃-TiO₂ was obtained by direct hydrolysis of titanium isopropoxide (sol-gel method) in previously synthesized WO₃ nanoparticles (6 mol% of WO₃), forming a composite that provided direct contact between WO₃ and TiO₂ nanoparticles. Subsequently, 0.5 wt% of copper or 0.5 wt% of palladium loadings was deposited onto WO₃-TiO₂. The photocatalytic hydrogen production results show that the activity increased with the presence of Cu and Pd species, reaching hydrogen production rates of 1496 μmol g⁻¹ h⁻¹ and 5427.07 μmol g⁻¹ h⁻¹ for Cu/WT and Pd/WT, respectively, as compared to WT structure (770.10 μmol g⁻¹ h⁻¹). To understand this behavior, semiconducting properties of the synthesized materials were characterized by (photo)electrochemical techniques. The presence of Cu and Pd in the structure moved the flatband position, increased the photocurrent and modified the open circuit potential under illumination toward less negative values, indicating the formation of energy states in the interface between WO₃-TiO₂ and the co-catalysts. These energy states at the heterojunction allow the transfer of photogenerated electrons toward co-catalysts, preventing the recombination of photogenerated charge carriers.

Handling Editor: Kevin Jones.

Address correspondence to E-mail: divadql@gmail.com; rodolfo.zanella@icat.unam.mx

<https://doi.org/10.1007/s10853-020-05188-z>

GRAPHIC ABSTRACT



Introduction

Developing renewable clean energy is an approach to solve the global energy crisis, and photocatalytic production of hydrogen is considered one of them [1]. TiO_2 is a semiconductor widely used in photocatalysis due to its high chemical stability, low cost and nontoxic nature [2]. However, it provides low photocatalytic efficiency due to the high recombination of photogenerated electron-hole pairs (e^-h^+) [3, 4].

Therefore, coupling TiO_2 with other metal oxides has been employed as a strategy to mitigate the recombination of (e^-h^+). In this sense, tungsten trioxide (WO_3) is an important semiconductor due to

the variety of its applications as electrochromic device, gas sensor and photocatalyst [5]. The construction of an efficient coupling of TiO_2 with WO_3 generates a favorable band alignment at the WO_3 – TiO_2 interface that allows charge separation [5–8]. However, it is important to ensure good contact between WO_3 – TiO_2 oxides, creating pathways for (e^-h^+) separation and improvement in the photocatalytic behavior of raw materials. In our previous work, M_xO_y (ZnO or SnO_2)– TiO_2 structures with different M_xO_y : TiO_2 molar ratios (01:99, 03:97, 06:94, 12:88, and 20:80) were obtained by sol–gel method, forming a composite that provided intimate contact between M_xO_y and TiO_2 by direct hydrolysis of titanium isopropoxide over previously synthesized M_xO_y nanoparticles, and the maximum photocatalytic

activity was observed for 6 mol% of M_xO_y [9–11]. The analysis performed by means of photoelectrochemical techniques showed that the interaction between M_xO_y - TiO_2 using this synthesis method provokes the formation of energy states at the interface of M_xO_y - TiO_2 that improve the (e^- - h^+) separation [9–11]. On the other hand, in order to obtain a good photocatalytic hydrogen evolution, besides separating the (e^- - h^+), it is necessary to create active sites for the reduction reaction. So, co-catalysts are needed to improve the reduction and oxidation process on the surface of a photocatalyst [11].

For this, the impregnation method can be used to synthesize supported photocatalysts with different co-catalysts since it is faster, inexpensive and in the case of low content of co-catalyst, allows the control of its dispersion on the surface. For example, some researchers have recently found that impregnation of TiO_2 with Cu species had a satisfactory photocatalytic activity for H_2 evolution, improving the charge carrier separation and providing the active sites for hydrogen production [12–15]. Ni et al. reported that low Cu content improved hydrogen production since these metallic nanoparticles are highly dispersed on the TiO_2 surface [16]. Chen et al. informed that low CuO loading on TiO_2 showed the best performance for hydrogen generation since, at higher CuO contents, agglomerations are formed, causing the detriment of photocatalytic activity [17]. Also, Pd species have been used in conjunction with TiO_2 for photocatalytic reactions in order to improve the water reduction process. Wu et al. reported an improved hydrogen production due to a synergistic effect between TiO_2 and Pd. Pd nanoparticles are considered to act as active reduction sites, while methanol acts as a sacrificial agent [18].

Hence, WO_3 - TiO_2 was synthesized with 6 mol% of WO_3 by the sol-gel method, creating a direct contact between these oxides to then deposit Cu or Pd species (0.5 wt%) onto the WO_3 - TiO_2 structure by impregnation method and evaluate its photocatalytic activity for hydrogen evolution. Photoelectrochemical performance studies of synthesized materials and their characterization allowed us to understand the effect of metallic nanoparticles on charge transfer processes and explain their photocatalytic behavior.

Experimental section

Reagents and chemicals

Sodium tungstate dihydrate (99% pure), dowex 50WX8 100–200 mesh, hydrochloric acid (37% pure), titanium isopropoxide (97% pure), isopropyl alcohol (99.9%), $Pd(NO_3)_2 \cdot 2H_2O$ (99.9% pure) and $Cu(NO_3)_2 \cdot 2.5H_2O$ (99.9% pure) were purchased from Sigma-Aldrich.

Milli-pore water with a resistivity of $18.2 \text{ M}\Omega \text{ cm}^{-1}$ was used to prepare all aqueous solutions.

Synthesis of WO_3 nanoparticles

Tungstate oxide nanoparticles were prepared by the ion-exchange resin method (Dowex 50WX8, 100–200 mesh). The ion-exchange resin (Dowex 50WX8, 100–200 mesh) was packed in a burette of 30 mL and activated with several washes of a concentrated HCl solution. Then, it was left in the HCl solution overnight to completely exchange the Na^+ by H^+ . After the ion-exchange resin activation, several washes were made with deionized water to eliminate excess HCl and the presence of Cl^- . Upon confirming the Cl^- elimination (silver nitrate test), a 0.1 M Na_2WO_4 solution was passed through the ion-exchange resin, producing a clear solution of tungstic acid with a pH ~ 1.8 . The solution was kept under stirring for 30 min. A yellow-white precipitate appeared within 5 h. Then, the precipitated solid was dried at 80°C for 24 h. Finally, the WO_3 nanoparticles were obtained when the solid was treated at 500°C for 2 h, using an air flow of 0.5 ml min^{-1} per milligram of photocatalyst (heating rate of $2^\circ \text{C min}^{-1}$).

Synthesis of WO_3 - TiO_2 structure

The WO_3 - TiO_2 structures were synthesized by the sol-gel technique based on the synthesis method previously reported by our research group [9–11]. The synthesis procedure was as follows: the WO_3 - TiO_2 structure with WO_3 6 mol% was achieved by adding 6 mol % of WO_3 nanoparticles (previously synthesized) to a solution with isopropyl alcohol and titanium isopropoxide in a 4:1 molar ratio under stirring. Then, to obtain full dispersion of WO_3 nanoparticles, the formed suspension was sonicated for 30 min, followed by stirring for a similar time period. A solution with isopropyl alcohol and

deionized water (1:1 molar ratio) was added to the suspension under stirring with the purpose of hydrolyzing isopropoxide over WO_3 nanoparticles. The suspension was then kept under stirring for 30 min to be homogenized. Finally, it was aged for 24 h and dried at 80 °C for another 24 h. The structure obtained, $\text{WO}_3\text{-TiO}_2$ (WT), was thermally treated at 350 °C for 2 h, using an H_2 flow of 0.5 ml min^{-1} per milligram of photocatalyst (heating rate of $2 \text{ }^\circ\text{C min}^{-1}$).

Synthesis of Pd–WT and Cu–WT structures

$\text{WO}_3\text{-TiO}_2$ (WT) structures, loaded with Pd and Cu (0.5 wt%) composites, were prepared by the incipient wetness impregnation (IWI) method. The WT composite was suspended in aqueous solutions of either $\text{Pd}(\text{NO}_3)_2 \cdot 2\text{H}_2\text{O}$ to obtain a 0.5 wt% load for Pd–WT or $\text{Cu}(\text{NO}_3)_2 \cdot 2.5\text{H}_2\text{O}$ to get a 0.5 wt% load for Cu–WT. The mixture was stirred for 16 h and dried at 80 °C for 8 h. Afterward, the dried photocatalysts were thermally treated at 300 °C for 2 h, using an H_2 flow of 0.5 ml min^{-1} per milligram of photocatalyst (heating rate of $2 \text{ }^\circ\text{C min}^{-1}$).

Characterization

X-ray diffractograms of the oxides were measured in air at room temperature using a Bruker D-8 Advance diffractometer with the Bragg–Brentano $\theta\text{-}\theta$ geometry, Cu $\text{K}\alpha$ radiation, a Ni 0.5% Cu- $\text{K}\beta$ filter in the secondary beam, and a one-dimensional position-sensitive silicon strip detector (Bruker, Lynxeye). The bandgap energies were calculated by a McLean analysis of the electronic spectra, which were obtained using a UV–visible Perkin-Elmer Lambda 40 spectrophotometer, equipped with an integrating sphere, and MgO used as a reference. Surface areas were measured by the BET method and were performed on an Autosorb-1 Quantachrome Instruments device.

The efficiency of Pd and Cu impregnation on the $\text{WO}_3\text{-TiO}_2$ structure was calculated by chemical analysis using inductively coupled plasma with optical emission spectrometry (ICP-OES) and Perkin-Elmer Optima 8300 equipment. Prior to analysis, samples were treated using microwave-assisted digestion in HCl at 175 °C.

XPS analyses were performed by a K-Alpha from Thermo Fisher Scientific X-ray photoelectron

spectrometer with a monochromatic Al $\text{K}\alpha$ X-ray source (1486.6 eV) and a base pressure of 1×10^{-9} Torr in the analytical chamber. The X-rays were microfocused at the source to project a spot size of 400 μm in diameter on the sample, using lenses in standard mode. The analyzer was run in constant analyzer energy (CAE) mode. Survey and high resolution spectra were collected using analyzer pass energies of 160 and 40 eV, respectively. The position of the adventitious oxygen O1s peak at 530.0 eV, from titanium oxide species, was monitored on each sample to ensure that no binding energy shift had occurred due to charging, associated with contact potential differences between the sample and the spectrometer. High resolution spectra were fitted using Gaussian–Lorentzian mix function and Shirley-type background subtraction. (Photo)electrochemical characterization was performed using the settings previously reported [9–11].

Photocatalytic hydrogen production

The photocatalytic activity of synthesized materials was evaluated in a borosilicate cylindrical photo-reactor with 200 mL of 90:10 water–methanol solution and 100 mg of the photocatalyst. The suspension was sonicated for 5 min and stirred in the dark for 30 min to disperse the photocatalyst; then, the dissolved air was displaced by bubbling nitrogen for 30 min. After bubbling with nitrogen, the light source was turned on. The light came from a UVP mercury lamp with primary emission at 254 nm (5.1 mW cm^{-2}), which was located inside a quartz tube at the center of the photo-reactor. A gas chromatograph (Agilent7820A) was used to determine the amount of H_2 that evolved over 7 h of the photoreaction. The GC device was equipped with an Agilent CP7429 column and a thermal conductivity detector. Argon was used as the carrier gas.

Results and discussion

Characterization of synthesized materials

The $\text{WO}_3\text{-TiO}_2$ structure (WT) was obtained by a sol-gel method developed by our research group [9–11]. The novelty of our approach consists in the use of previously synthesized WO_3 nanoparticles and their incorporation during TiO_2 formation. In this way,

intimate WO_3 - TiO_2 contact is ensured, creating pathways for electron-hole separation and improvement in the photocatalytic behavior of raw materials.

This was corroborated by carrying out TEM analysis of the WO_3 - TiO_2 nanoparticle system, Fig. 1a and b. The micrographs reveal the presence of agglomerate particles, possibly associated with a nonhomogeneous layer (grey zones), which surrounds dark zones related to cores, i.e., individual nanoparticles. However, these images did not permit differentiation or elucidation of the distribution between the WO_3 - TiO_2 nanoparticles. The usage of electron energy loss spectroscopy (EELS) mapping analysis allowed us to overcome this problem in Fig. 1b. The series of mapping spatial distribution images for W, Ti and W/Ti can be seen in Fig. 1c–e, respectively. From TEM and EELS mapping analyses, it was concluded that WO_3 nanoparticles were successfully coated with TiO_2 .

To gain more insight into the interfacial interaction between WO_3 - TiO_2 , the presence of co-catalysts (Cu and Pd), and the crystal structure of synthesized materials, high-resolution TEM (HRTEM) and XRD analyses were used. Figures 2a and b show the HRTEM of WO_3 - TiO_2 with Cu and Pd nanoparticles. In both figures, the interfacial interaction between WO_3 and TiO_2 nanoparticles can be clearly observed with the presence of interplanar distances 0.37, 0.38 and 0.26 nm corresponding to (0,2,0), (0,0,2) and

(2,2,0) monoclinic planes of WO_3 and 0.35 nm corresponding to the (1,0,1) anatase plane of TiO_2 [19–23]. These results are consistent with those observed in EELS-TEM (Fig. 1) and XRD analysis (Fig. 2c). For all synthesized materials, the monoclinic WO_3 phase (JCPDS No.83-950) with (0,0,2) preferred orientation was observed in Fig. 2c. This phase (monoclinic WO_3) is related to the calcination, at 500 °C, of the previously synthesized WO_3 nanoparticles before the formation of the WT structure, which gives this structure thermal stability [24, 25]. Likewise, the diffraction peaks of anatase phase (TiO_2 , JCPDS No.84-1286) were observed for all synthesized materials (Fig. 2c). Cu and Pd diffraction peaks are not detected in the XRD analysis, which can be attributed to the low content ($\sim 0.5\%$ wt) and thorough dispersion of co-catalysts on the WT surface. However, interplanar distances of 0.24 nm, corresponding to (1,1,1) cubic plane of Cu_2O (Fig. 2a), and 0.262, 0.238 and 0.224 nm corresponding to (1,0,1) plane of PdO and (1,1,1) plane of Pd metallic nanoparticles, can be observed in HRTEM images, as shown in Fig. 2a and b, respectively [26–29].

Chemical analysis using inductively coupled plasma with optical emission spectrometry (ICP-OES) was employed to determine the efficiency of the impregnation of co-catalysts (see Table 1). The results showed that the theoretical and real co-catalyst contents are very close to each other, confirming the

Figure 1 **a** TEM image WO_3 - TiO_2 (6 mol% WO_3). **b** TEM image of WO_3 - TiO_2 (6 mol% WO_3) and elemental mapping patterns of **c** W, **d** Ti and **e** for clarify the mapping points of W and Ti.

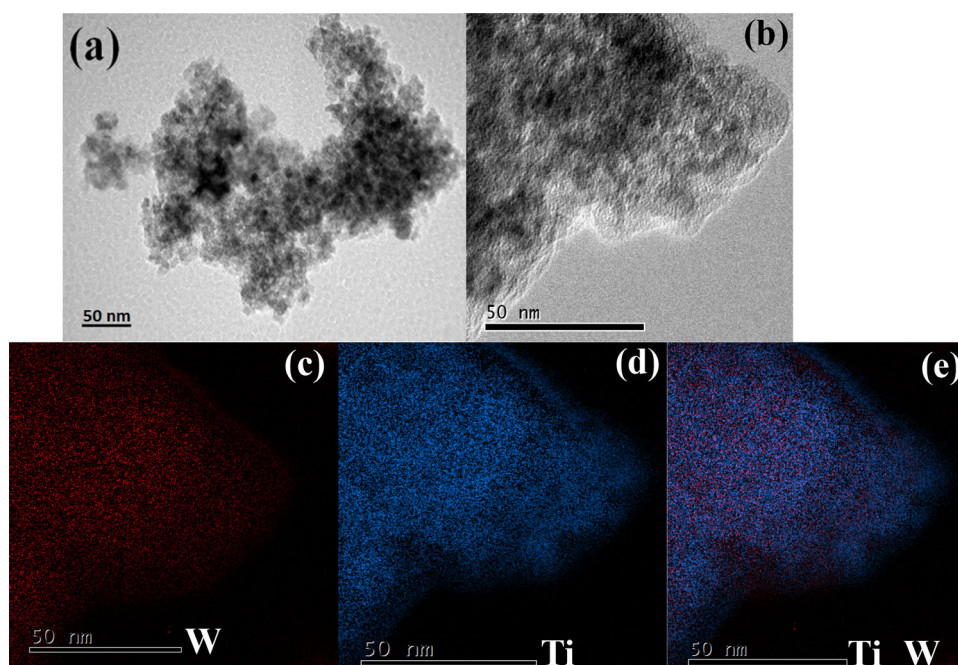


Figure 2 HR-TEM images of **a** $\text{WO}_3\text{-TiO}_2$ with 0.5 wt% of Cu and **b** $\text{WO}_3\text{-TiO}_2$ with 0.5 wt% of Pd and **c** XRD diffraction patterns of: (i) $\text{WO}_3\text{-TiO}_2$ (6 mol% WO_3), (ii) $\text{WO}_3\text{-TiO}_2$ with Cu 0.5% and (iii) $\text{WO}_3\text{-TiO}_2$ with Pd 0.5%.

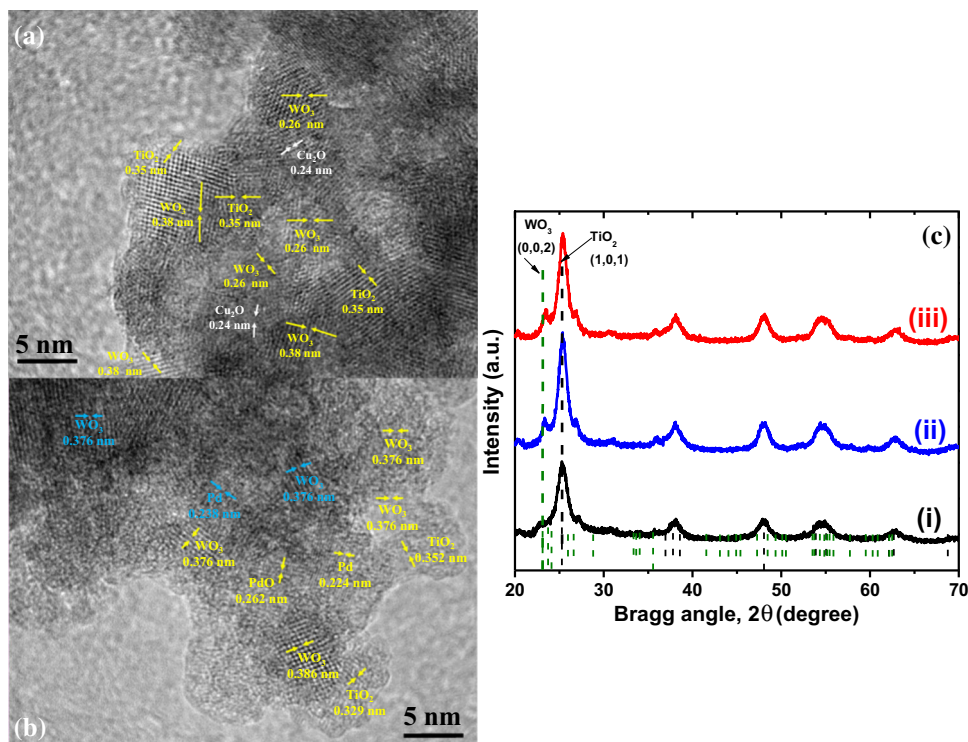


Table 1 Real wt% content of co-catalysts, specific surface area (BET method), average pore diameter (d_{pore}), pore volume (V_{pore}) and bandgap energies (E_g) of synthesized materials

Materials	Real content co-catalysts (wt%) ^a	S_{BET} ($\text{m}^2 \text{g}^{-1}$) ^b	d_{pore} (nm) ^b	V_{pore} ($\text{cm}^3 \text{g}^{-1}$) ^b	E_g (eV) ^c
$\text{WO}_3\text{-TiO}_2$	–	267	9.12	0.43	3.33
0.5wt%Cu-WT	0.47	168	14.46	0.37	3.25
0.5wt%Pd-WT	0.60	177	13.38	0.37	3.23

^aEstimated by ICP-OES

^bEstimated by the BET method of N_2 adsorption

^cEstimated by UV–vis diffuse reflectance spectroscopy

effective impregnation of the metal precursors onto $\text{WO}_3\text{-TiO}_2$ (WT).

The HRTEM and ICP-OES results confirm the presence of Cu and Pd species on WT, and interfacial interaction between co-catalysts and the base material (WT) is observed, which leads to an improvement in the photocatalytic performance.

Also, the textural properties of synthesized materials were measured by N_2 adsorption–desorption isotherms to evaluate the effect of Cu and Pd impregnation on the WT structure. The specific surface area values (Table 1), calculated by the BET method, show that Cu-WT and Pd-WT systems exhibit a lower specific surface area than the WT

pristine material. However, they are high enough to perform oxidation and reduction reactions on the photocatalyst surface. These results suggest that copper and palladium co-catalysts are well dispersed on the surface of the WT material [30–32].

On the other hand, UV–vis diffuse reflectance spectroscopy (DRS) was used to evaluate the optical properties of synthesized materials to obtain more information about the effect of Cu and Pd on the WT structure. The UV–vis spectra in Fig. 3a show an adsorption edge at ~ 373 nm for the WT structure, characteristic of tetrahedral symmetry of Ti^{4+} in TiO_2 , the material present in large proportion [33, 34]. Furthermore, the WT structure showed no absorption

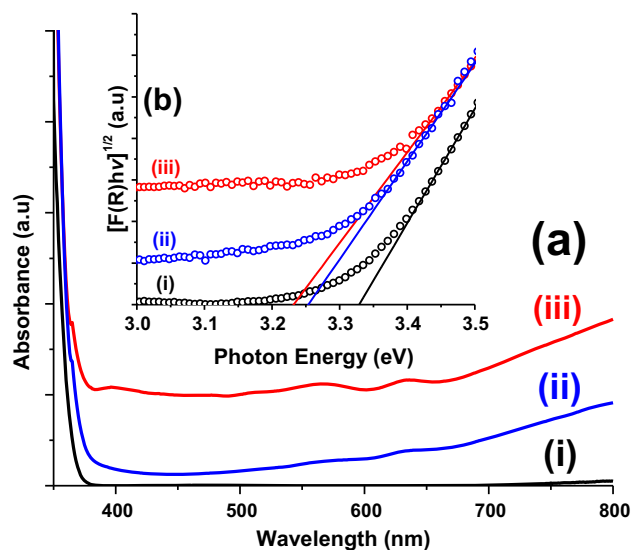


Figure 3 **a** UV-vis spectra of: (i) WO₃-TiO₂, (ii) WO₃-TiO₂ with 0.5 wt% of Cu and (iii) WO₃-TiO₂ with 0.5 wt% of Pd and **b** Insert of schematic presentation of the McLean analysis of the absorption edge for determining the bandgap energy (E_g) of: (i) WO₃-TiO₂, (ii) WO₃-TiO₂ with 0.5 wt% of Cu and (iii) WO₃-TiO₂ with 0.5 wt% of Pd.

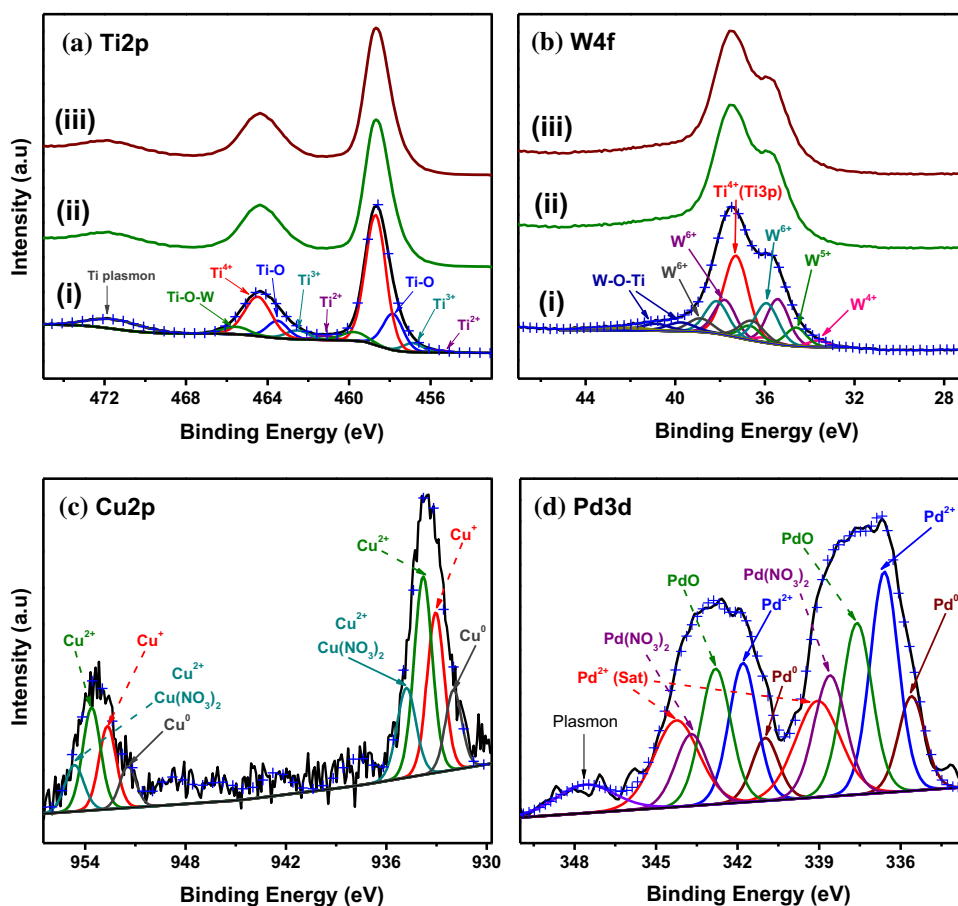
in the visible region. However, the modification of WT with Cu and Pd nanoparticles caused a significant increase in the absorption in this region. In the same way, the absorptions at around 560 and 630 nm, attributed to a damping effect caused by $d-d$ interband transitions, originated from copper species in the case of Cu-WT material and from palladium species in the case of Pd-WT material [26, 35, 36]. A schematic presentation of the McLean analysis of the absorption edge, used to determine the band gap energy of the synthesized materials, is shown in Fig. 3b. The bandgap energy of WT with co-catalysts shifted slightly toward lower energy compared to the base material (WT), implying that copper and palladium species were not doped into the lattice structure of WO₃ or TiO₂ but highly dispersed on the WT surface, which confirms the results observed in HRTEM and textural properties. The bandgap energy values (E_g) of the synthesized materials are summarized in Table 1.

The surface electronic state and composition of the chemical species involved in the charge transfer process during photocatalytic hydrogen production were explored by performing high resolution X-ray photoelectron spectroscopy in all the synthesized materials and those thermally treated in hydrogen. Thus, in the narrow scan corresponding to the

bonding energies for the Ti2p region, titanium was identified in three different oxidation states (Fig. 4a). A weak peak centered at 461.2 and 455.6 ± 0.2 eV corresponds to Ti 2p_{1/2} and Ti 2p_{3/2}, respectively, related to the presence of Ti²⁺ species. In addition, the peaks centered at 462.5 and 456.9 ± 0.2 eV corresponding to Ti 2p_{1/2} and Ti 2p_{3/2}, respectively, indicate the presence of Ti³⁺ species in the form of Ti₂O₃ [37, 38]. Ti²⁺ and Ti³⁺ species are a signature of oxygen vacancy defects in the structure, associated with the thermal treatment in hydrogen. On the other hand, the typical bonding of Ti-O at 457.8 and 463.5 ± 0.2 eV, related to Ti⁴⁺ species in the structure, is discerned. Similarly, the major TiO₂ contribution in the structure (~ 94%) with oxidation state Ti⁴⁺ exhibited the characteristic bonding energies at 458.6 and 464.4 ± 0.2 eV [37–40]. Moreover, the peaks centered at 459.7 and 465.5 ± 0.2 eV are related to the formation of Ti-O-W bonds, which confirms the chemical environment composed of TiO₂ and WO₃, and indicates a strong interaction between them [41, 42].

The narrow scan corresponding to the bonding energies for the W4f region revealed a multi-contribution (Fig. 4b). The major contribution corresponds to Ti3p at 37.2 ± 0.2 eV due to Ti⁴⁺ species in anatase TiO₂ phase [43, 44]. Likewise, tungsten was identified in three different oxidation states. A weak double contribution, centered at 36.0 and 33.6 ± 0.2 eV corresponds to W4f_{5/2} and W4f_{7/2}, respectively, related to W⁴⁺ species [45]. Additionally, the peaks centered at 36.6 and 34.6 ± 0.2 eV correspond to W4f_{5/2} and W4f_{7/2}, indicating the presence of W⁵⁺ species [45, 46]. As observed in the titanium region, the presence of W⁵⁺ and W⁴⁺ species is correlated with oxygen vacancies due to the hydrogen thermal treatment. Furthermore, the peaks centered at 37.7 and 35.4 ± 0.2 eV are related by W atoms to oxidation state + 6 [46, 47]. Besides, the contributions observed at 38.1 and 35.9 ± 0.2 eV correspond to W4f_{5/2} and W4f_{7/2}, and the peaks centered at 38.8 and 36.5 ± 0.2 eV are attributed to W⁶⁺ species related to the typical W-O bonding present in WO₃ and a residue of the H₂WO₄ precursor used during the synthesis process [48]. Moreover, the contribution to higher binding energies at 40.8 and 39.7 ± 0.2 eV is attributed to the formation of W-O-Ti surface bonds, in agreement with the Ti-O-W contribution detected in the Ti2p region, which confirms a strong interaction between them [41].

Figure 4 XPS high-resolution spectra of **a** Ti2p high resolution of: (i) WO₃-TiO₂, (ii) WO₃-TiO₂ with 0.5 wt% of Cu and (iii) WO₃-TiO₂ with 0.5 wt% of Pd, **b** W4f high resolution of: (i) WO₃-TiO₂, (ii) WO₃-TiO₂ with 0.5 wt% of Cu and (iii) WO₃-TiO₂ with 0.5 wt% of Pd, **c** Cu2p high resolution of WO₃-TiO₂ with 0.5 wt% of Cu and **d** Pd3d high resolution of WO₃-TiO₂ with 0.5 wt% of Pd.



Meanwhile, the Cu2p spectrum (Fig. 4c) was decomposed into four different chemical species. The smallest contribution is associated with metallic copper (Cu⁰), located at 951.4 and 931.9 ± 0.2 eV, corresponding to Cu2p_{1/2} and Cu2p_{3/2}, respectively. However, metallic copper corresponds to similar binding energy values as Cu⁺ observed at 952.6 and 933.0 ± 0.2 eV, Cu2p_{1/2} and Cu2p_{3/2}, respectively, and these oxidation states are generally difficult to distinguish from XPS analysis of the Cu2p region [49, 50]. On the other hand, the main contribution of Cu species is in the form of Cu²⁺ dispersed on the surface of the WT structure, whose peaks Cu2p_{1/2} and Cu2p_{3/2} are located at 953.6 and 933.8 ± 0.2 eV, respectively. Additionally, the gap between these two energy levels is about ~ 20 eV, which is a strong indication of the CuO presence [51–53]. The double contribution, detected at 954.6 and 934.8 ± 0.2 eV, to Cu2p_{1/2} and Cu2p_{3/2}, respectively, corresponds to Cu(NO₃)₂ remnants of the impregnation process [53]. Finally, the characteristic copper multi-component satellites were observed at higher binding energies

(941–946 eV). It is important to point out that the impregnation of Cu does not modify titanium and tungsten species in the WT structure [see Fig. 4a(ii) and b(ii)].

Pd3d core level spectra are shown in Fig. 4d. After fitting the experimental data, the characteristic metallic Pd binding energies were identified at 340.9 and 335.6 ± 0.2 eV for Pd3d_{3/2} and Pd3d_{5/2} peaks. The gap between these two energy levels is about ~ 5.3 eV, confirming the presence of metallic Pd nanoparticles dispersed on the surface of the WT structure [54, 55]. The second double contribution, associated with the Pd3d_{3/2} and Pd3d_{5/2}, at 341.8 and 336.5 eV, is assigned to the Pd²⁺ species [56]. The thermal treatment in a hydrogen atmosphere (at 300 °C for 2 h, using an H₂ flow of 0.5 ml min⁻¹ per milligram of photocatalyst, with a heating rate of 2 °C min⁻¹) causes the formation of PdO in several steps. As a result, at low binding energies (336.5 eV), PdO nanoparticles with low crystallinity are obtained [57]. However, other contributions at 342.8 and 337.6 ± 0.2 eV for Pd3d_{3/2} and Pd3d_{5/2} peaks are

related to the formation of well-crystallized PdO nanoparticles [57]. It is important to mention that the use of a reducing atmosphere does not allow the formation of Pd^{4+} in the form of PdO_2 since this chemical species is highly unstable [58]. On the other hand, the contribution detected at 343.7 and 338.6 ± 0.2 eV for $\text{Pd}3d_{3/2}$ and $\text{Pd}3d_{5/2}$ peaks is related to Pd^{2+} species in the form of $\text{Pd}(\text{NO}_3)_2$ as a residue of the impregnation process [59]. Finally, the characteristic satellites were observed at 344.2 and 339.0 ± 0.2 eV for $\text{Pd}3d_{3/2}$ and $\text{Pd}3d_{5/2}$ related to Pd^{2+} species [57, 60]. As in the case of Cu, the impregnation of Pd species does not modify the species of titanium and tungsten present in the WT structure [see Fig. 4a(iii) and b(iii)].

Photocatalytic evaluation of hydrogen production

The performance of synthesized materials was evaluated for the photocatalytic hydrogen production from methanol–water mixtures (10:90 methanol:water) under UV irradiation, with a low concentration of sacrificial agent (methanol), compared to the normally used 1:1 methanol–water volume ratio.

First, we have investigated the H_2 production without photocatalyst under UV light irradiation (photolysis), as a function of time reaction, which is shown in Fig. 5a(i). As can be observed, the hydrogen amount increases progressively during the reaction, reaching $63.03 \mu\text{mol}$ at 6 h, which can be translated as a hydrogen production rate of $10.50 \mu\text{mol h}^{-1}$. In the case of pristine materials, WO_3 and TiO_2 , thermally treated in a reducing atmosphere [Fig. 5a(ii) and (iii)], the hydrogen production rate was 391.33 and $510.11 \mu\text{mol g}^{-1} \text{h}^{-1}$, respectively, being almost 37 and 48 times higher than the H_2 production by photolysis (see Fig. 5b). Also, when the WO_3 – TiO_2 structure is tested, a higher hydrogen production rate ($770.10 \mu\text{mol g}^{-1} \text{h}^{-1}$) than with the pristine materials is obtained. This value is 1.5 times higher than that measured when using TiO_2 (thermally treated in a reducing atmosphere), see Fig. 5b.

When WO_3 and TiO_2 are coupled with the synthesis method used in this work, intimate contact and strong interaction are generated between them, as observed in the HRTEM and XPS analyses. This interaction creates a synergistic effect on photocatalytic hydrogen production. Similarly, the formation of oxygen vacancies (mixed-valance) due to the

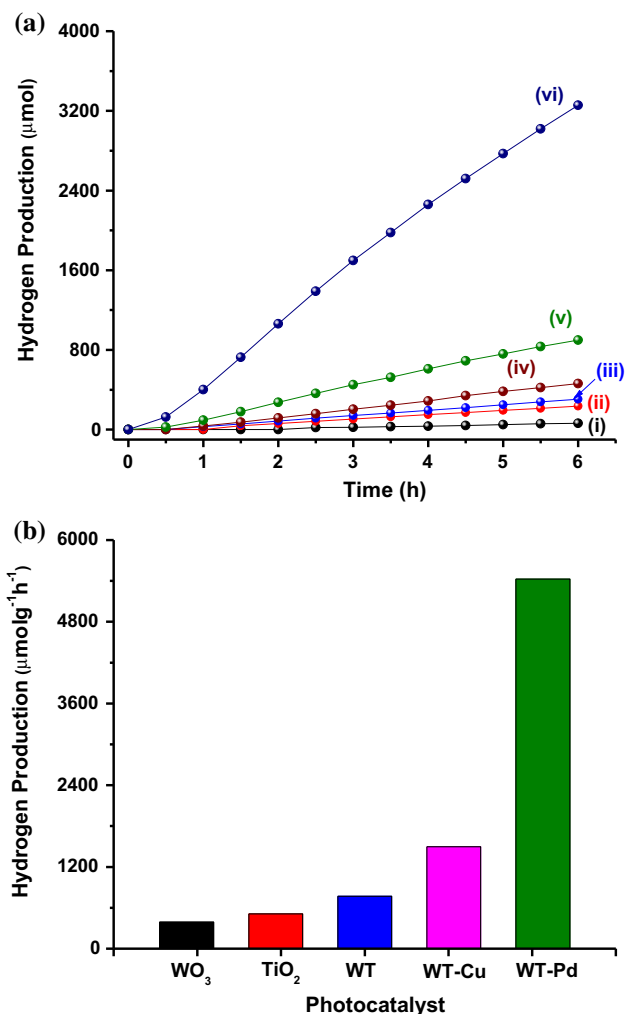


Figure 5 a Hydrogen production of synthesized materials: (i) photolysis, (ii) WO_3 , (iii) TiO_2 , (iv) WO_3 – TiO_2 , (v) WO_3 – TiO_2 with 0.5 wt% Cu and (vi) WO_3 – TiO_2 with 0.5 wt% Pd (UV light irradiation measured in methanol–water mixture 10:90), b Hydrogen production rate of synthesized materials as a function of the reaction time (UV light irradiation measured in methanol–water mixture 10:90).

reducing atmosphere during heat treatment helps to generate surface and/or energy states at the WO_3/TiO_2 interface, which prevent the recombination of charge carriers, as discussed in detail in previous studies [11, 61].

On the other hand, the photocatalytic activity toward hydrogen production is enhanced in the presence of co-catalysts (Cu or Pd species) compared to the WT structure (Fig. 5a and b). This can be associated with n – p interaction as expected, causing a better separation of the charge carriers. When co-catalysts are loaded on WT, the photogenerated

electrons can be rapidly transported to Cu or Pd nanoparticles, which have been spotted as active sites for the hydrogen evolution reaction from water reduction. Analogously, photogenerated holes are removed by methanol that acts as a hole scavenger [62]. Although the co-catalyst content loaded was almost the same in both cases (for Cu and Pd), the activity drastically varied; the hydrogen production rate was 5427.07, 1496.39 and 770.10 $\mu\text{mol g}^{-1} \text{h}^{-1}$ for Pd/WO₃-TiO₂, Cu/WO₃-TiO₂, and WO₃-TiO₂, respectively. These results may be attributed to the properties of the different metals, such as surface energy, redox potential and the modification of the chemical environment and its interaction with the components of the solution [63].

It is worth mentioning that the Pd/WO₃-TiO₂ performance enhanced 7 times the activity of the WO₃-TiO₂ structure. Moreover, on comparing the photocatalytic activity and stability of Pd and Cu loaded on WT structure in successive cycles (Fig. 6), the hydrogen production yield is found to decrease after 3 re-use cycles. For instance, the photocatalytic activity of Cu/WO₃-TiO₂ and Pd/WO₃-TiO₂ decreased by 9.7 and 15.2%, respectively. This decrease in the photocatalytic activity must be associated with various factors. It is well known that palladium species are active in the methanol oxidation reaction. However, their photocatalytic functions for methanol conversion differ drastically from copper species. For example, Pd metallic nanoparticles for methanol reforming produce mostly the decomposition products CO and H₂ [64, 65]. In a previous study with the Au-Pd/TiO₂ material in our laboratory, after several hydrogen reaction cycles, a band was identified at 2088 cm^{-1} in the FTIR CO adsorption experiment, attributed to the adsorption of CO on metallic Pd nanoparticles [66]. These results give clear proof that both CO selectivity and hydrogen production rates are higher over Pd species than over Cu species under the same reaction conditions. Therefore, the decrease in photocatalytic activity could be due to CO adsorbed on the surface of co-catalysts, which disrupts the interactions between the WT structure and co-catalysts (Pd and Cu species), provoking a decrease in the H₂ production yield. However, it is important to point out that hydrogen production in these materials was still much higher than the activity of the WT structure, being almost 2 and 6 times higher for Cu/WO₃-TiO₂ and Pd/WO₃-TiO₂, respectively.

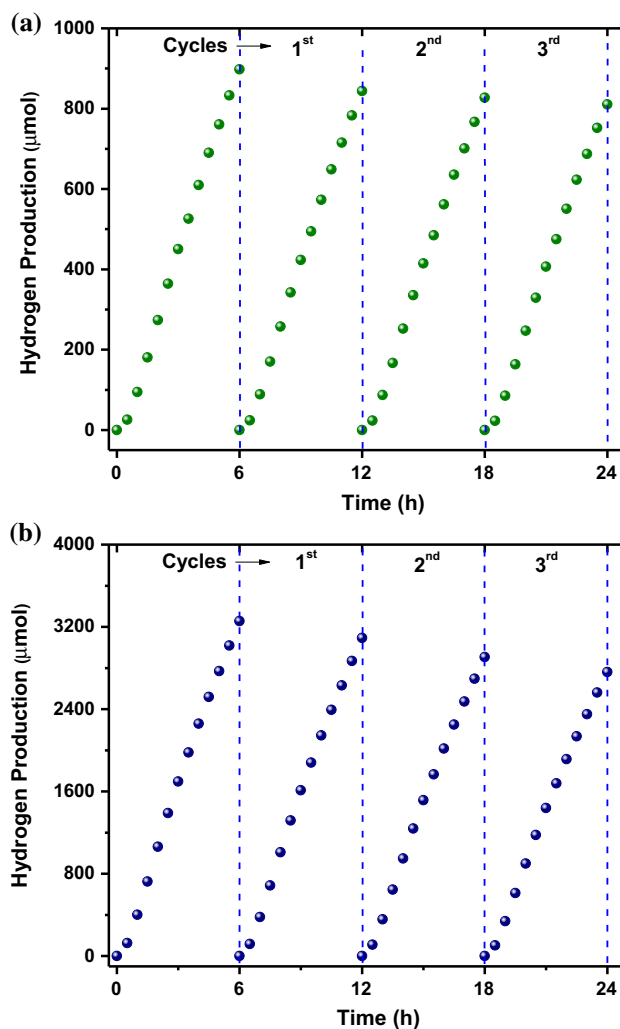


Figure 6 Reuse cycles of: **a** WO₃-TiO₂ with 0.5 wt% Cu and **b** WO₃-TiO₂ with 0.5 wt% Pd material in the photocatalytic hydrogen production (UV light irradiation measured in methanol-water mixture 10:90).

(Photo)electrochemical characterization, band alignment and determination of energy states

To gain a deeper understanding of the photocatalytic performance of the synthesized materials and the charge transfer process between *n-p* heterojunctions, the semiconducting properties of these materials were estimated from Mott-Schottky curves (Figure S1. Supplementary Information). The flatband potential (E_{fb}) of the synthesized materials was estimated by extrapolating the linear region, formed in C_{SC}^{-2} versus potential curves, to the potential axis. The values of E_{fb} estimated for all synthesized materials are shown in Table 2.

Table 2 The flatband potential (E_{fb}) of the synthesized materials

Materials	E_{fb} versus (Ag/AgCl/3 M KCl) (V)
WO ₃	− 0.76
TiO ₂	− 0.71
WO ₃ –TiO ₂	− 0.87
0.5wt%Cu–WT	− 0.73
0.5wt%Pd–WT	− 0.94

WO₃ and TiO₂ exhibited an *n*-type behavior with a positive slope in the linear region of C_{SC}^{-2} versus potential curve; the values of E_{fb} here obtained for WO₃ and TiO₂ are − 0.76 V and − 0.71 V, respectively. When WO₃ and TiO₂ are coupled with this synthesis method, the E_{fb} displaces toward more negative values (Table 2); this effect has been observed in previous studies with different composite materials and is related to the energy states generated at grain boundaries between oxides that directly impact the charge transfer through the interface, as sketched in Fig. 7a [9–11].

Contrastingly, when Cu species are coupled with the WT structure, the E_{fb} value of the composite becomes less negative (see Fig. 7b) due to the Fermi level alignment through the composite. On the other hand, the WT structure modified with Pd species exhibits the most negative E_{fb} value among the composites (Fig. 7c), which means that the photo-generated electron will have a more reducing capacity, i.e., a more negative potential to perform the hydrogen evolution reaction from water. It should be noted that base materials and WT with co-catalysts exhibited a higher E_{fb} than the potential for hydrogen evolution reaction [− 0.62 V versus Ag/AgCl (3.0 M KCl) at neutral pH], showing that all synthesized materials meet the minimal thermodynamic requirements to perform the water reduction (see Fig. 7).

In addition, photoelectrochemical experiments were performed to study the photoinduced electron transfer process at the interface between WT and the co-catalysts (Cu and Pd species) under illumination and its impact on hydrogen production. The photocurrent responses of the WT structure with and

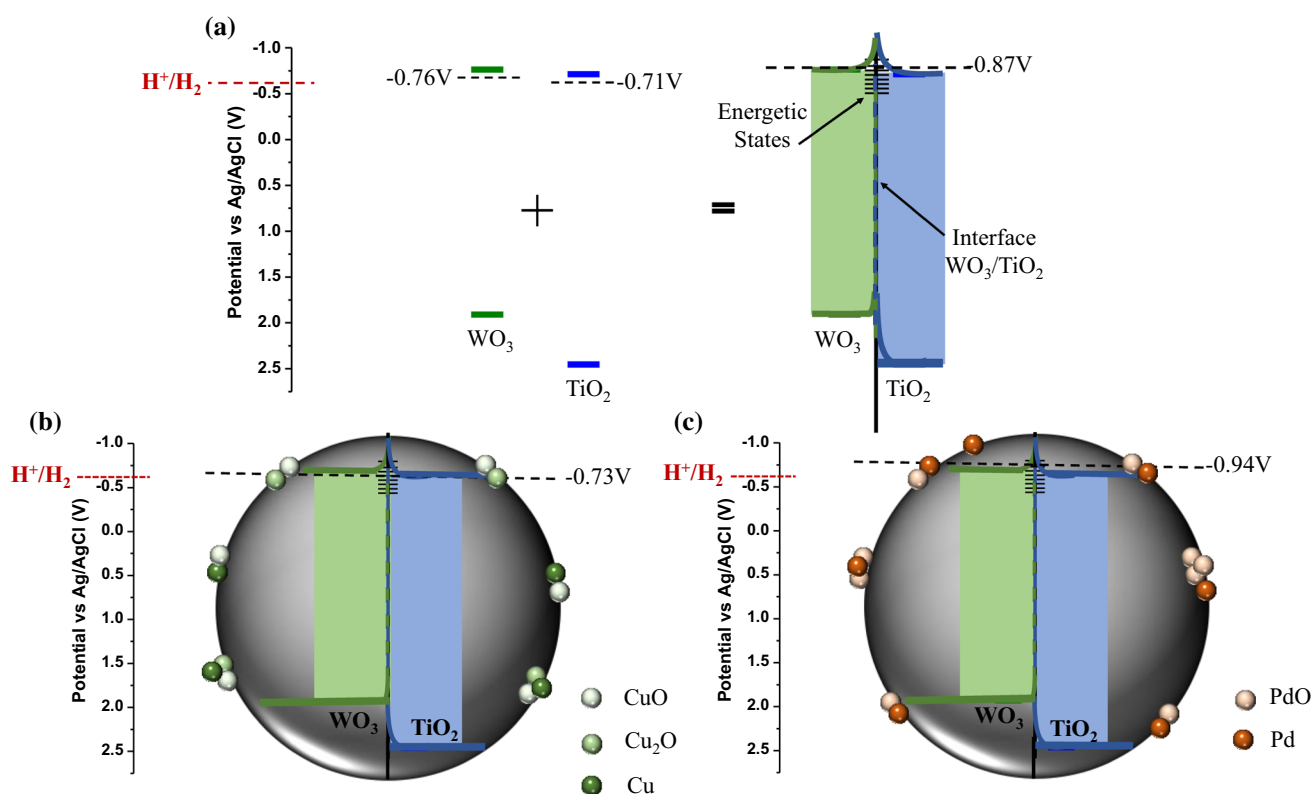


Figure 7 a Energy scheme of base materials (WO₃, TiO₂) and their interaction in WO₃–TiO₂ structure. The band energy position was estimated from flatband potentials (E_{fb}) (Table 2) and bandgap

energy (E_g) (Table 1) and WO₃–TiO₂ structure and the interaction with: **b** Cu species and **(c)** Pd species.

without the co-catalyst are shown in Fig. 8a. Initially, the current was measured at 0.5 V versus Ag/AgCl bias voltage for 60 s to stabilize the current in the dark. Then, the film with the synthesized material was illuminated for another 60 s, causing an increase in the recorded current. After that, the light was interrupted again, causing the currents to decrease rapidly until reaching their value in the dark.

The photocurrent is generated by several consecutive steps such as photon absorption by TiO₂ and WO₃, charge separation favored by the creation of heterojunction, the presence of co-catalysts and transport of photogenerated electrons through the film toward the current collector, favored by the

potential differences imposed for the measurement. Meanwhile, holes are rapidly transported to the semiconductor/electrolyte interface to perform the methanol or water oxidation process.

Figure 8a shows that the film with the WT structure exhibited the lowest photocurrent. However, the addition of Cu and Pd co-catalysts enhanced the photocurrent mainly due to a more efficient charge separation promoted by them. The presence of both co-catalysts could facilitate methanol and water oxidation processes. The considerably larger photocurrent measured in the presence of Pd can be attributed to the combination of two effects related to improved charge separation and a surface with higher catalytic activity to promote the charge transfer at the electrode/electrolyte interface.

Besides, open circuit potential (OCP) measurements were performed for WT, WT-Cu and WT-Pd structures. The effect of illumination on the OCP as a function of time is shown in Fig. 8b.

When the films containing the synthesized materials were illuminated (WT with and without co-catalyst), the OCP began to change toward more negative values (typical of *n*-type semiconductors). This behavior indicates the accumulation of the photogenerated electrons in the conduction band or/and energy levels located below it (Fig. 8b). By interrupting the illumination of the films, the OCP slightly changed toward less negative values but moved in the opposite direction when the films were illuminated again. This behavior proves the stability of the electron accumulation process in the films (Fig. 8b).

Significant changes are observed in the response of Cu-WT and Pd-WT structures under illumination compared to the base WT structure. The structures with the presence of co-catalysts reach less negative OCP values, showing a slower response to reach a stable value of OCP under illumination [Fig. 8b(ii) and (iii)]. This delay in reaching a stable OCP is normally related to the filling of energy states with lower energy, probably generated at the co-catalysts-WT interface. These energy states can act as electron traps, improving the separation of the charge carriers. As seen in Fig. 8b, the material with the slowest and most unstable response to on/off intervals is the structure with Pd species. This behavior can be attributed to the fact that Pd species are well dispersed on the WT structure, contributing to a quicker separation and transfer of electrons to the solution.

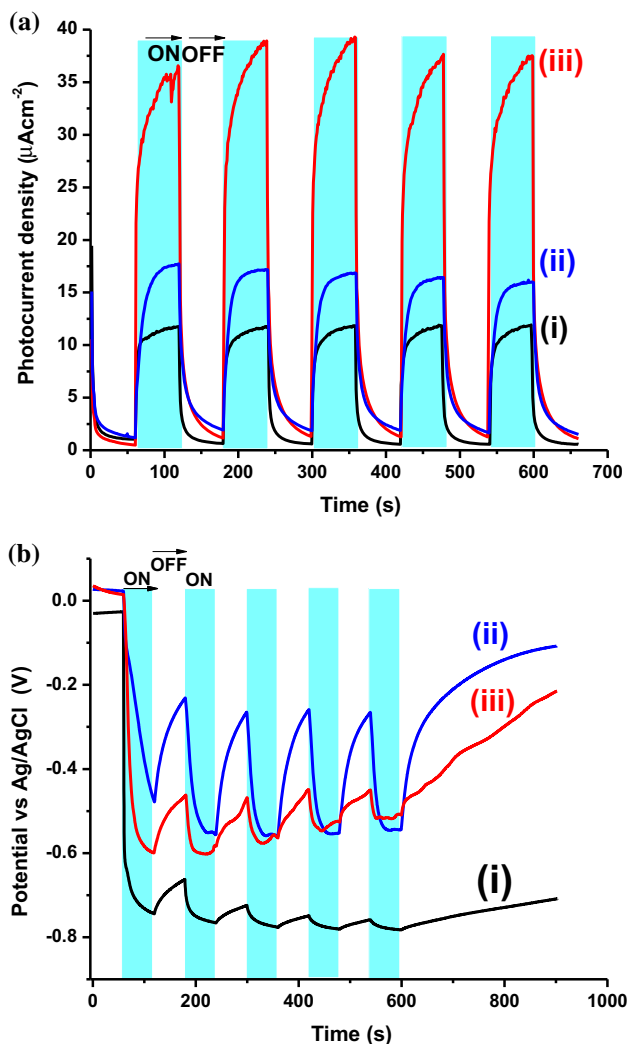
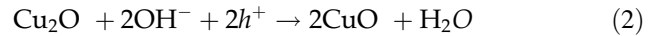


Figure 8 Photoelectrochemical characterization of photocatalyst: (i) WO₃-TiO₂, (ii) WO₃-TiO₂ with Cu species and (iii) WO₃-TiO₂ with Pd species: **a** photocurrent versus time and **b** photovoltage versus time.

So, the presence of a co-catalyst improves the photocatalytic hydrogen production, which is confirmed by photoelectrochemical analysis.

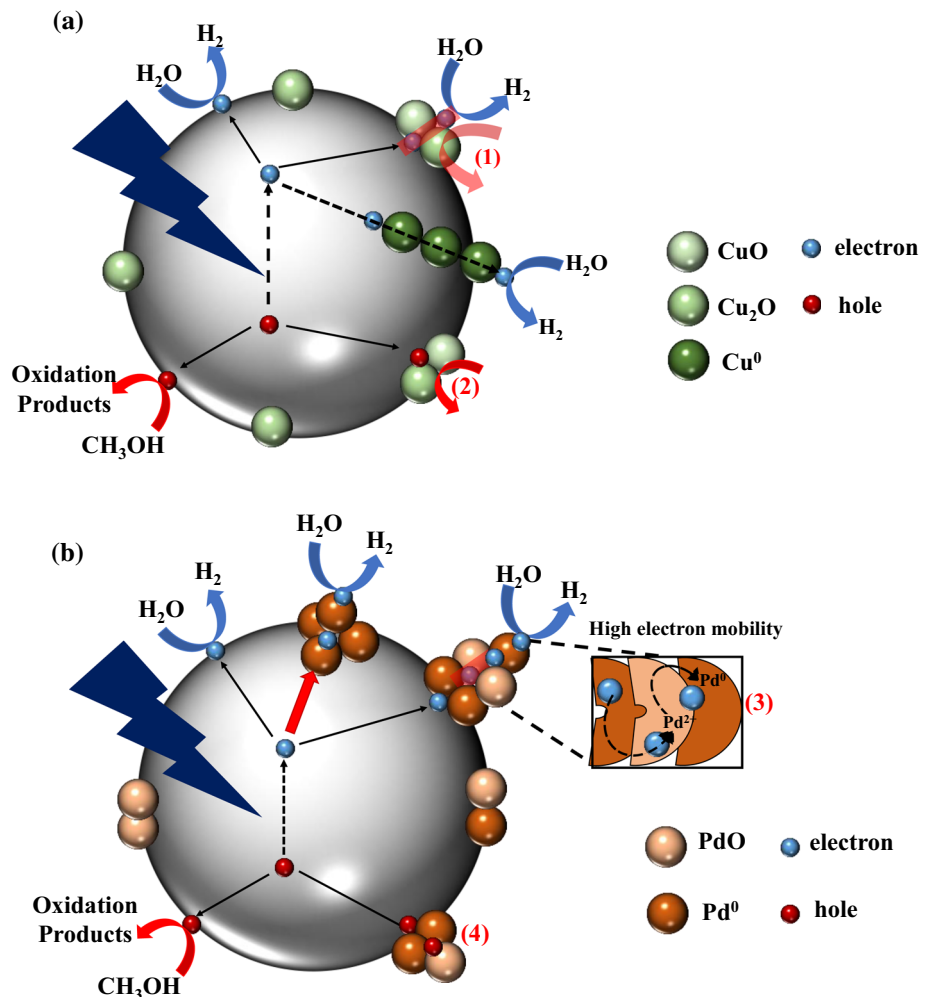
Therefore, the interaction between co-catalysts and the WT structure has been discussed as follows. After irradiation with UV light of WT with Cu species on the surface, the photogenerated electrons are separated across the entire structure and can take two paths: (1) migrate to the surface and carry out the water reduction process or (2) migrate to the copper nanoparticles (see Scheme 1a). In this second path, the electrons can be rapidly transferred with the help of the copper species on the surface and catalyze hydrogen production or/and reduce Cu^{2+} to Cu^+ (see Scheme 1a and Reaction 1) [11]. The Cu^+ species can be reoxidized to Cu^{2+} by the holes photogenerated in CuO or WT structure (see Scheme 1a and Reaction 2) [11]. Moreover, the existence of metallic copper nanoparticles in the WT structure helps to

improve the transport and conductivity of electrons, thereby increasing their photocatalytic activity and catalyzing hydrogen production [11].

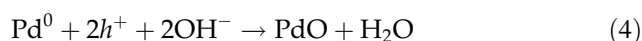
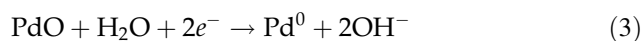


In the case of WT with Pd species on the surface, after irradiation with UV light, the photogenerated electrons are separated and can take three paths: (1) migrate to the WT surface and carry out the water reduction process, (2) migrate to metallic Pd nanoparticles, improving the transport and conductivity of electrons and catalyzing hydrogen production or (3) migrate to the surface of WT and reduce PdO nanoparticles (Pd^{2+}) in situ into Pd^0 (see Scheme 1b and Reaction 3). Once Pd^0 is reduced to Pd^0 , this metallic nanoparticle promotes the high photocatalytic activity by generating a Schottky

Scheme 1 Schematic representation of the charge transfer in: **a** WT structure with Cu species for photocatalytic hydrogen production and **b** WT structure with Pd species for photocatalytic hydrogen production.



junction between the metal and the WT structure. It can trap, store and transport the photogenerated electrons reducing the rate of the ($e^- - h^+$) recombination [32, 67].



Also, metallic Pd nanoparticles deposited onto WT can be reoxidized by photogenerated holes (see Scheme 1b and Reaction 4).

To sum up, all of the experimental evidence provided in this research sheds light on the effect of Cu and Pd species loading on $\text{WO}_3\text{-TiO}_2$ that occurs during the photocatalytic hydrogen production under UV light. The EELS-TEM and HRTEM analyses show the intimate contact and interfacial interaction between WO_3 and TiO_2 . Similarly, HRTEM shows the interaction between Cu and Pd co-catalysts with $\text{WO}_3\text{-TiO}_2$, where a uniform distribution around the WT structure is observed, causing a decrease in the surface area. The XRD characterization shows that there are no considerable structural changes in the WT matrix associated with the treatment used to load Cu and Pd by the incipient wetness impregnation method, which is related to their uniform dispersion and low concentration.

The XPS analysis shows the chemical environment and the species that participate in the charge transfer process during the production of photocatalytic hydrogen. This technique allowed us to observe a strong interaction between WO_3 and TiO_2 generated by the sol-gel method used. The presence of mixed-valence titanium, tungsten and co-catalyst species is also observed. These mixed-valence compounds in the structure generate defects in the material by creating energy states at the interface, thus modifying its semiconducting properties. Therefore, the determination of semiconducting properties by photoelectrochemical techniques, when WO_3 and TiO_2 are coupled, reveals that E_{fb} of the structure becomes more negative than that of the pristine materials (see Table 2), due to the generation of energy states at the interface. These states can behave as shallow energy states to separate the charge carriers, and thus provide a path for electron transfer toward the co-catalysts and improve the photocatalytic activity.

The addition of Cu and Pd increases the ($e^- - h^+$) separation, mobility and transfer of the electrons to the solution for the reduction of water to hydrogen, obtaining the best performance for the Pd/WT structure.

Conclusion

The sol-gel synthesis method, used in this work, allowed TiO_2 nanoparticles to grow on the previously synthesized WO_3 nanoparticles, generating direct contact between them and thus allowing the formation of a heterojunction. The dispersion of Cu and Pd species onto the surface of WT material causes a decrease in the surface area and creates additional defect states in the optical properties. HRTEM and XPS experiments showed a strong interaction at the interface of TiO_2 and WO_3 . The photocatalytic activity for H_2 evolution shows that the use of Cu and mainly Pd species over $\text{WO}_3\text{-TiO}_2$ favors hydrogen production due to the fact that Cu and Pd species improve the charge carrier separation process, acting as co-catalysts and increasing the transfer of electrons to the solution. The presence of Cu and Pd in the structure, moved the flatband position increased the photocurrent, and changed the open-circuit potential under illumination toward less negative values, indicating the formation of energy states at the interface between $\text{WO}_3\text{-TiO}_2$ and co-catalysts. These energy states at the heterojunction act as traps during the photocatalytic process, preventing the recombination of photogenerated charge carriers.

Acknowledgements

The authors would like to thank the financial support provided by Consejo Nacional de Ciencia y Tecnología (CONACYT) through the CB-18269 Grant and Dirección General de Asuntos del Personal Académico-UNAM through the PAPIIT IN103719 Grant. We also thank the Laboratorio Universitario de Caracterización Espectroscópica (LUCE-UNAM) and the Laboratorio Universitario de Nanotecnología Ambiental (LUNA-UNAM) and the technical support provided by Viridiana Maturano Rojas and

Selene Islas Sánchez, David A. Ramírez Ortega (CVU 329398) thanks CONACYT postdoctoral Grant.

Compliance with ethical standards

Conflict of interest The authors declare that contents of this work have not conflict of interest with any individual or organization.

Electronic supplementary material: The online version of this article (<https://doi.org/10.1007/s10853-020-05188-z>) contains supplementary material, which is available to authorized users.

References

- [1] Liu G, Kolodziej C, Jin R, Qi S, Lou Y, Chen J, Jiang D, Zhao Y, Burda C (2020) MoS₂-Stratified CdS-Cu_{2-x}S core-shell nanorods for highly efficient photocatalytic hydrogen production. *ACS Nano* 14:5468–5479. <https://doi.org/10.1021/acsnano.9b09470>
- [2] Lu M, Shao C, Wang K, Lu N, Zhang X, Zhang P, Zhang M, Li X, Liu Y (2014) p-MoO₃ nanostructures/n-TiO₂ nanofiber heterojunctions: controlled fabrication and enhanced photocatalytic properties. *ACS Appl Mater Interfaces* 6(12):9004–9012. <https://doi.org/10.1021/am5021155>
- [3] McCullagh C, Skillen N, Adams M, Robertson PKJ (2011) Photocatalytic reactors for environmental remediation: a review. *J Chem Technol Biotechnol* 86:1002–1017. <https://doi.org/10.1002/jctb.2650>
- [4] Chan SHS, Wu TY, Juan JC, The CY (2011) Recent developments of metal oxide semiconductors as photocatalysts in advanced oxidation processes (AOPs) for treatment of dye waste-water. *J Chem Technol Biotechnol* 86:1130–1158. <https://doi.org/10.1002/jctb.2636>
- [5] Pan Hong J, Lee in W, (2006) Preparation of highly ordered cubic mesoporous WO₃/TiO₂ films and their photocatalytic properties. *Chem Mater* 18:847–853. <https://doi.org/10.1021/cm0522782>
- [6] Rey A, García-Muñoz P, Hernández-Alonso MD, Mena E, García-Rodríguez S, Beltrán FJ (2014) WO₃-TiO₂ based catalysts for the simulated solar radiation assisted photocatalytic ozonation of emerging contaminants in a municipal wastewater treatment plant effluent. *Appl Catal B Environ* 154–155:274–284. <https://doi.org/10.1016/j.apcatb.2014.02.035>
- [7] Toledo Camacho SY, Rey A, Hernández-Alonso MD, Llorca J, Medina F, Contreras S (2018) Pd/TiO₂-WO₃ photocatalysts for hydrogen generation from water-methanol mixtures. *Appl Surf Sci* 455:570–580. <https://doi.org/10.1016/j.apsusc.2018.05.122>
- [8] DohLeviL-MitroviL Z, StojadinoviL S, Lozzi L, AškraBiL S, RosiL M, TomiL N, PaunoviL N, LazoviL S, NikoliL-Santucci MGS (2016) WO₃/TiO₂ composite coatings: structural, optical and photocatalytic properties. *Mater Res Bull* 83:217–224. <https://doi.org/10.1016/j.materresbull.2016.06.011>
- [9] Ramírez-Ortega D, Meléndez AM, Acevedo-Peña P, González I, Arroyo R (2014) Semiconducting properties of ZnO/TiO₂ composites by electrochemical measurements and their relationship with photocatalytic activity. *Electrochim Acta* 140:541–549. <https://doi.org/10.1016/j.electacta.2014.06.060>
- [10] Ramírez-Ortega D, Acevedo-Peña P, Tzompantzi F, Arroyo R, González F, González I (2017) Energetic states in SnO₂-TiO₂ structures and their impact on interfacial charge transfer process. *J Mater Sci* 52:260–275. <https://doi.org/10.1007/s10853-016-0328-3>
- [11] Guerrero-Araque D, Acevedo-Peña P, Ramírez-Ortega D, Lartundo-Rojas L, Gómez R (2017) SnO₂-TiO₂ structures and the effect of CuO, CoO metal oxide on photocatalytic hydrogen production. *J Chem Technol Biotechnol* 92:1531–1539. <https://doi.org/10.1002/jctb.5273>
- [12] Lalitha K, Sadanandam G, Kumari VD, Subrahmanyam M, Sreedhar B, Hebalkar NY (2010) Highly stabilized and finely dispersed Cu₂O/TiO₂: a promising visible sensitive photocatalyst for continuous production of hydrogen from glycerol: water mixtures. *J Phys Chem C* 114:22181–22189. <https://doi.org/10.1021/jp107405u>
- [13] Li L, Xu L, Shi W, Guan J (2013) Facile preparation and size-dependent photocatalytic activity of Cu₂O nanocrystals modified titania for hydrogen evolution. *Int J Hydrog Energy* 38:816–822. <https://doi.org/10.1016/j.ijhydene.2012.10.064>
- [14] Lo SS, Mirkovic T, Chuang C-H, Burda C, Scholes GD (2011) Emergent properties resulting from type-II band alignment in semiconductor nanoheterostructures. *Adv Mater* 23:180–197. <https://doi.org/10.1002/adma.201002290>
- [15] Wang Y, Zhang Y, Zhao G, Tian H, Shi H, Zhou T (2012) Design of a novel Cu₂O/TiO₂/carbon aerogel electrode and its efficient electrosorption-assisted visible light photocatalytic degradation of 2,4,6-trichlorophenol. *ACS Appl Mater Interfaces* 4:3965–3972. <https://doi.org/10.1021/am300795w>
- [16] Ni D, Shen H, Li H, Ma Y, Zhai T (2017) Synthesis of high efficient Cu/TiO₂ photocatalysts by grinding and their size-dependent photocatalytic hydrogen production. *Appl Surf Sci* 409:241–249. <https://doi.org/10.1016/j.apsusc.2017.03.046>
- [17] Chen W-T, Jovic V, Sun-Waterhouse D, Idriss H, Waterhouse GIN (2013) The role of CuO in promoting

- photocatalytic hydrogen production over TiO₂. *Int J Hydrog Energy* 38:15036–15048. <https://doi.org/10.1016/j.ijhydene.2013.09.101>
- [18] Wu J, Lu S, Ge D, Zhang L, Chen W, Gu H (2016) Photocatalytic properties of Pd/TiO₂ nanosheets for hydrogen evolution from water splitting. *RSC Adv* 6:67502–67508. <https://doi.org/10.1039/C6RA10408H>
- [19] Vuong NM, Kim D, Kim H (2013) Electrochromic properties of porous WO₃-TiO₂ core-shell nanowires. *J Mater Chem C* 1:3399–3407. <https://doi.org/10.1039/C3TC30157E>
- [20] Patil SM, Deshmukh SP, More KB, Shevale VB, Mullani SB, Dhodamani AG, Delekar SD (2019) Sulfated TiO₂/WO₃ nanocomposite: an efficient photocatalyst for degradation of Congo red and methyl red dyes under visible light irradiation. *Mater Chem Phys* 225:247–255. <https://doi.org/10.1016/j.matchemphys.2018.12.041>
- [21] Wei Y, Huang Y, Fang Y, Zhao Y, Luo D, Guo Q, Fan L, Wu J (2019) Hollow mesoporous TiO₂/WO₃ sphere heterojunction with high visible-light-driven photocatalytic activity. *Mater Res Bull* 119:110571–110578. <https://doi.org/10.1016/j.materresbull.2019.110571>
- [22] Mathankumar G, Bharathi P, Mohan MK, Harish S, Navaneethan M, Archana J, Suresh P, Mani GK, Dhivya P, Ponnusamy S, Muthamizhchelvan C (2020) Synthesis and functional properties of nanostructured Gd-doped WO₃/TiO₂ composites for sensing applications. *Mater Sci Semicond Process* 105:104732–104740. <https://doi.org/10.1016/j.mssp.2019.104732>
- [23] Prabhu S, Cindrella L, Kwon OJ, Mohanraju K (2019) Photoelectrochemical, photocatalytic and photochromic performance of rGO-TiO₂-WO₃ composites. *Mater Chem Phys* 224:217–228. <https://doi.org/10.1016/j.matchemphys.2018.12.030>
- [24] Ke D, Li H, Peng T, Liu X, Ke D (2008) Preparation and photocatalytic activity of WO₃/TiO₂ nanocomposite particles. *Mater Lett* 62:447–450. <https://doi.org/10.1016/j.matlet.2007.05.060>
- [25] Ramana CV, Utsunomiya S, Ewing RC, Julien CM, Becker U (2006) Structural stability and phase transitions in WO₃ thin films. *J Phys Chem B* 110:10430–10435. <https://doi.org/10.1021/jp056664i>
- [26] Mondal I, Pal U (2016) Synthesis of MOF templated Cu/CuO@TiO₂ nanocomposites for synergistic hydrogen production. *Phys Chem Chem Phys* 18:4780–4788. <https://doi.org/10.1039/C5CP06292F>
- [27] Zhen W, Jiao W, Wu Y, Jing H, Lu G (2017) The role of a metallic copper interlayer during visible photocatalytic hydrogen generation over a Cu/Cu₂O/Cu/TiO₂ catalyst. *Catal Sci Technol* 7:5028–5037. <https://doi.org/10.1039/C7CY01432E>
- [28] Yuan J, Zhang J-J, Yang M-P, Meng W-J, Wang H, Lu J-X (2018) CuO Nanoparticles supported on TiO₂ with high efficiency for CO₂ electrochemical reduction to ethanol. *Catalysts* 8:171–181. <https://doi.org/10.3390/catal8040171>
- [29] Zhao Q, Li H, Zhang L, Cao Y (2019) Study of PdO species on surface of TiO₂ for photoreduction of CO₂ into CH₄. *J Photochem Photobiol A* 384:112032–112039. <https://doi.org/10.1016/j.jphotochem.2019.112032>
- [30] Dong X, Ma X, Xu H, Ge Q (2016) Comparative study of silicasupported copper catalysts prepared by different methods: formation and transition of copper phyllosilicate. *Catal Sci Technol* 6:4151–4158. <https://doi.org/10.1039/C5CY01965F>
- [31] Rungjaroentawon N, Onsuratoom S, Chavadej S (2012) Hydrogen production from water splitting under visible light irradiation using sensitized mesoporous-assembled TiO₂-SiO₂ mixed oxide photocatalysts. *Int J Hydrog Energy* 37:11061–11071
- [32] Rusinque B, Escobedo S, de Lasa H (2020) Photoreduction of a Pd-doped mesoporous TiO₂ photocatalyst for hydrogen production under visible light. *Catalysts* 10:74–97. <https://doi.org/10.3390/catal10010074>
- [33] López R, Gómez R, Llanos ME (2010) Photophysical and photocatalytic properties of nanosized copper-doped titania sol-gel catalysts. *Catal Today* 148:103–108. <https://doi.org/10.1016/j.cattod.2009.04.001>
- [34] Chen J, Lin L-B, Jing F-Q (2001) Theoretical study of F-type color center in rutile TiO₂. *J Phys Chem Solids* 62:1257–1262. [https://doi.org/10.1016/S0022-3697\(01\)00018-X](https://doi.org/10.1016/S0022-3697(01)00018-X)
- [35] Yu H, Irie H, Hashimoto K (2010) Conduction band energy level control of titanium dioxide: toward an efficient visible-light-sensitive photocatalyst. *J Am Chem Soc* 132:6898–6899. <https://doi.org/10.1021/ja101714s>
- [36] Wu Y, Lu G, Li S (2009) The role of Cu(I) species for photocatalytic hydrogen generation over CuO_x/TiO₂. *Catal Lett* 133:97–105. <https://doi.org/10.1007/s10562-009-0165-y>
- [37] Mekasuwandumrong O, Chaitaworn S, Panpranot J, Praserttham P (2019) Photocatalytic liquid-phase selective hydrogenation of 3-nitrostyrene to 3-vinylaniline of various treated-TiO₂ without use of reducing gas. *Catalysts* 9:329–343. <https://doi.org/10.3390/catal9040329>
- [38] Kumar Paul K, Jana S, Giri PK (2018) Tunable and high photoluminescence quantum yield from self-decorated TiO₂ quantum dots on fluorine doped mesoporous TiO₂ flowers by rapid thermal annealing. *Part Part Syst Char* 35:1800198–1800213. <https://doi.org/10.1002/ppsc.201800198>

- [39] Zakrzewska K (2012) Nonstoichiometry in TiO_{2-y} studied by ion beam methods and photoelectron spectroscopy. *Adv Mater Sci Eng* 826873:1–13. <https://doi.org/10.1155/2012/826873>
- [40] Kato K, Xin Y, Shirai T (2019) Structural-controlled synthesis of highly efficient visible light TiO_2 photocatalyst via one-step single-mode microwave assisted reaction. *Sci Rep* 9:4900–49008. <https://doi.org/10.1038/s41598-019-41465-x>
- [41] Grandcolas M, Cottineau T, Louvet A, Keller N, Keller V (2013) Solar light-activated photocatalytic degradation of gas phase diethylsulfide on WO_3 -modified TiO_2 nanotubes. *Appl Catal B Environ* 138–139:128–140. <https://doi.org/10.1016/j.apcatb.2013.02.041>
- [42] Gao L, Gan W, Qiu Z, Zhan X, Qiang T, Li J (2017) Preparation of heterostructured WO_3/TiO_2 catalysts from wood fibers and its versatile photodegradation abilities. *Sci Rep* 7:1102–1114. <https://doi.org/10.1038/s41598-017-01244-y>
- [43] Chang F, Wang J, Luo J, Sun J, Deng B, Hu X (2016) Enhanced visible-light-driven photocatalytic performance of mesoporous W-Ti-SBA-15 prepared through a facile hydrothermal route. *Colloid Surf A* 499:69–78. <https://doi.org/10.1016/j.colsurfa.2016.04.013>
- [44] Patrocínio AOT, Paula LF, Paniago RM, Freitas J, Bahnenmann DW (2014) Layer-by-layer TiO_2/WO_3 thin films as efficient photocatalytic self-cleaning surfaces. *ACS Appl Mater Interfaces* 6:16859–16866. <https://doi.org/10.1021/am504269a>
- [45] Terohid SAA, Heidari S, Jafari A (2018) Effect of growth time on structural, morphological and electrical properties of tungsten oxide nanowire. *Appl Phys A* 124:567–575. <http://doi.org/10.1007/s00339-018-1955-0>
- [46] Alonso-Tellez A, Robert D, Keller V, Keller N (2014) H₂S photocatalytic oxidation over WO_3/TiO_2 Hombikat UV100. *Environ Sci Pollut Res* 21:3503–3514. <https://doi.org/10.1007/s11356-013-2329-y>
- [47] Gui Y, Blackwood DJ (2014) Electrochromic enhancement of WO_3 - TiO_2 composite films produced by electrochemical anodization. *J Electrochem Soc* 161:E191–E201. <https://doi.org/10.1149/2.0631414jes>
- [48] Reale F, Palczynski P, Amit I, Jones GF, Mehew JD, Bacon A, Ni N, Sherrell PC, Agnoli S, Craciun MF, Russo S, Mattev C (2017) High-mobility and high-optical quality atomically thin WS_2 . *Sci Rep* 7:14911–14920. <https://doi.org/10.1038/s41598-017-14928-2>
- [49] Drouet C, Laberty C, Fierro JLG, Alphonse P, Rousset A (2000) X-ray photoelectron spectroscopic study of non-stoichiometric nickel and nickel-copper spinel manganites. *J Inorg Mater* 2:419–426. [https://doi.org/10.1016/S1466-6049\(00\)00047-7](https://doi.org/10.1016/S1466-6049(00)00047-7)
- [50] Monte M, Munuera G, Costa D, Conesa JC, Martínez-Arias A (2015) Near-ambient XPS characterization of interfacial copper species in ceria-supported copper catalysts. *Phys Chem Chem Phys* 17:29995–30004. <https://doi.org/10.1039/C5CP04354A>
- [51] Mohammad A, Chandra P, Ghosh T, Carraro M, Mobin SM (2017) Facile access to amides from oxygenated or unsaturated organic compounds by metal oxide nanocatalysts derived from single-source molecular precursors. *Inorg Chem* 56:10596–10608. <https://doi.org/10.1021/acs.inorgchem.7b01576>
- [52] Richharia P, Chopra KL, Bhatnagar MC (1991) Surface analysis of a black copper selective coating. *Sol Energy Mater* 23:93–109. [https://doi.org/10.1016/0165-1633\(91\)90156-F](https://doi.org/10.1016/0165-1633(91)90156-F)
- [53] Biesinger MC (2017) Advanced analysis of copper X-ray photoelectron spectra. *Surf Interface Anal* 49:1325–1334. <https://doi.org/10.1002/sia.6239>
- [54] Tressaud A, Khairoun S, Touhara H, Watanabe N (1986) X-ray photoelectron spectroscopy of palladium fluorides. *Chemie* 540–541:291–299. <https://doi.org/10.1002/zaac.19865400932>
- [55] Priolkar KR, Bera P, Sarode PR, Hegde MS, Emura S, Kumashiro R, Lalla NP (2002) Formation of $\text{Ce}_{1-x}\text{Pd}_x\text{O}_{2-\delta}$ solid solution in combustion-synthesized Pd/CeO₂ catalyst: XRD, XPS, and EXAFS investigation. *Chem Mater* 14:2120–2128. <https://doi.org/10.1021/cm0103895>
- [56] Cai G, Luo W, Xiao Y, Zheng Y, Zhong F, Zhan Y, Jiang L (2018) Synthesis of a highly stable Pd@CeO₂ catalyst for methane combustion with the synergistic effect of urea and citric acid. *ACS Omega* 3:16769–16776. <https://doi.org/10.1021/acsomega.8b02556>
- [57] Kibis LS, Titkov AI, Stadnichenko AI, Koscheev SV, Boronin AI (2009) X-ray photoelectron spectroscopy study of Pd oxidation by RF discharge in oxygen. *Appl Surf Sci* 255:9248–9254. <https://doi.org/10.1016/j.apsusc.2009.07.011>
- [58] Moroseac M, Skála T, Veltruská K, Matolín V, Matolínová I (2004) XPS and SSIMS studies of Pd/SnO_x system: reduction and oxidation in hydrogen containing air. *Surf Sci* 566–568:1118–1123. <https://doi.org/10.1016/j.susc.2004.06.068>
- [59] Tan H-Z, Wang Z-Q, Xu Z-N, Sun J, Chen Z-N, Chen Q-S, Chen Y, Guo G-C (2017) Active Pd(II) complexes: enhancing catalytic activity by ligand effect for carbonylation of methyl nitrite to dimethyl carbonate. *Catal Sci Technol* 7:3785–3790. <https://doi.org/10.1039/C7CY01305A>
- [60] Veziroglu S, Hwang J, Drewes J, Barg I, Shondo J, Strunskus T, Polonskyi O, Faupel F, Aktas OC (2020) PdO

- nanoparticles decorated TiO₂ film with enhanced photocatalytic and self-cleaning properties. *Mater Today* 16:100251. <https://doi.org/10.1016/j.mtchem.2020.100251>
- [61] Guerrero-Araque D, Acevedo-Peña P, Ramírez-Ortega D, Calderon HA, Gómez R (2017) Charge transfer processes involved in photocatalytic hydrogen production over CuO/ZrO₂-TiO₂ materials. *Int J Hydrog Energy* 42:9744–9753. <https://doi.org/10.1016/j.ijhydene.2017.03.050>
- [62] Sreethawong T, Yoshikawa S (2005) Comparative investigation on photocatalytic hydrogen evolution over Cu-, Pd-, and Au-loaded mesoporous TiO₂ photocatalysts. *Catal Commun* 6:661–668. <https://doi.org/10.1016/j.catcom.2005.06.004>
- [63] Xu C, Wang X, Zhu J (2008) Graphene–metal particle nanocomposites. *J Phys Chem C* 112:9841–19845. <https://doi.org/10.1021/jp807989b>
- [64] Agrell J, Hasselbo K, Jansson K, Järåsa G, S, Boutonnet M, (2001) Production of hydrogen by partial oxidation of methanol over Cu/ZnO catalysts prepared by microemulsion technique. *Appl Catal A Gen* 211:239–250. [https://doi.org/10.1016/S0926-860X\(00\)00876-0](https://doi.org/10.1016/S0926-860X(00)00876-0)
- [65] Agrell J, Germani G, Järås SG, Boutonnet M (2003) Production of hydrogen by partial oxidation of methanol over ZnO-supported palladium catalysts prepared by microemulsion technique. *Appl Catal A Gen* 242:233–245. [https://doi.org/10.1016/S0926-860X\(02\)00517-3](https://doi.org/10.1016/S0926-860X(02)00517-3)
- [66] Barrios CE, Albiter E, Gracia y Jimenez J.M., Tiznado H, Romo-Herrera J, Zanella R, (2016) Photocatalytic hydrogen production over titania modified by gold–metal (palladium, nickel and cobalt) catalysts. *Int J Hydrog Energy* 41:23287–23300. <https://doi.org/10.1016/j.ijhydene.2016.09.206>
- [67] Bahruji H, Bowker M, Davies PR, Morgan DJ, Morton CA, Egerton TA, Kennedy J, Jones W (2015) Rutile TiO₂-Pd photocatalysts for hydrogen gas production from methanol reforming. *Top Catal* 58:70–76. <https://doi.org/10.1007/s11244-014-0346-9>

Publisher's Note Springer Nature remains neutral with regard to jurisdictional claims in published maps and institutional affiliations.